Journal of Catalysis 266 (2009) 182–190

Contents lists available at ScienceDirect

Journal of Catalysis

journal homepage: www.elsevier.com/locate/jcat

Reversible changes in the Pt oxidation state and nanostructure on a ceria-based supported Pt

Miho Hatanaka *, Naoki Takahashi, Naoko Takahashi, Toshitaka Tanabe, Yasutaka Nagai, Akihiko Suda, Hirofumi Shinjoh

TOYOTA Central R&D Labs., Inc., 41-1 Yokomichi, Nagakute, Nagakute-cho, Aichi-gun, Aichi 480-1192, Japan

ARTICLE INFO

Article history:
Received 18 March 2009
Revised 12 May 2009
Accepted 8 June 2009

Keywords:
Platinum
Ceria
Automotive catalyst
X-ray photoelectron spectroscopy
Transmission electron microscopy

ABSTRACT

The Pt oxidation state and nanostructure on a ceria-based oxide support were characterized after sequential oxidative, reductive, and re-oxidative treatments using X-ray photoelectron spectroscopy and transmission electron microscopy. The Pt oxidation state and nanostructure depended on the treatment atmosphere: an oxidized Pt monolayer spread along the primary particle surface of the ceria-based oxide support in the oxidized catalyst, whereas metallic Pt existed as particles of 1–2 nm in diameter in the reduced catalyst. Therefore, on the ceria-based oxide surface oxidized Pt formed a nanocomposite oxide with Ce under an oxidative atmosphere and reversibly changed to metallic Pt particles under a reductive atmosphere. The formation of this surface nanocomposite oxide is evidence of the strong interaction between oxidized Pt and CeO_2 that involves the formation of a Pt–O–Ce bond, which stabilizes Pt against sintering and redisperses agglomerated Pt particles under an oxidative atmosphere.

1. Introduction

In the mid-1970s, three-way catalysts (TWCs) were first used in the US and Japan to convert harmful carbon monoxide (CO), nitrogen oxides (NO_x), and hydrocarbons (HC) in the exhaust from gasoline-fueled vehicles to harmless carbon dioxide (CO_2), nitrogen (N_2), and water (H_2O) [1]. TWC-equipped exhausts are now widely used in gasoline-fueled vehicles to meet stringent emission regulations. The main components in TWCs are a precious metal such as palladium (Pd), platinum (Pt), or rhodium (Rh) as the active catalyst, an inorganic oxide such as γ-alumina (Al_2O_3) or zirconia (ZrO_2) as the support, and an oxygen storage material such as ceria–zirconia (CeO_2–ZrO_2) to maintain stoichiometry at the catalyst surface and achieve higher purification activity [2–4]. Because of the scarcity of natural resources and the increasing price of precious metals, there is a focus on improving the durability of TWCs and applying new insights to develop advanced TWCs with lower precious metal content [5–14].

In principle, when the particle size of a precious metal increases due to sintering during the lifetime of a catalyst, the TWC activity deteriorates [15]. Sintering of precious metal particles has been widely investigated, with some researchers focusing on preventing sintering on aging [2,16–29]. CeO_2-based inorganic oxides are well known as good supports for stabilization of Pt particles against sintering, whereas Pt easily agglomerates on Al_2O_3 under an oxidative atmosphere at high temperature [2,26–29].

We obtained novel insights into the mechanism by which CeO_2-based oxide supports stabilize Pt against sintering in a systematic atomic-level investigation using X-ray absorption fine structure (XAFS) methodology [27]. Curve fitting of the Pt L_3-edge extended X-ray absorption fine structure (EXAFS) spectrum of an air-aged catalyst revealed a strong interaction between oxidized Pt and CeO_2-based support involving a rigid Pt–O–Ce bond that stabilized Pt atoms under an oxidative atmosphere at high temperature. From the coordination number of Pt–O and Pt–Ce shells estimated from EXAFS analysis, it could be concluded that this Pt–O–Ce bond was formed at the surface of the support and not in the bulk. A similar Pt–O–Ce surface complex on a CeO_2-based oxide support was reported by Diwell et al. [28] and Murrell et al. [29]. We also systematically evaluated interaction between Pt and supports after air aging by X-ray photoelectron spectroscopy (XPS), X-ray absorption near edge structure (XANES), and CO adsorption [27]. Our results revealed that a more basic support yielded better Pt stabilization through the formation of rigid Pt–O–M (where M is the support cation) bonds, thus inhibiting Pt sintering.

In another in situ time-resolved XAFS investigation [30,31], we found that the Pt–O–Ce bond formed under an oxidative atmosphere at high temperature acted as the driving force for redispersion of sintered Pt particles into smaller particles. Previously sintered Pt particles on a CZY support were redispersed as small particles on treatment in an oxidative atmosphere at 873 K. Such Pt redispersion did not occur on an Al_2O_3 support. In situ TEM

* Corresponding author. Fax: +81 561 636150.
E-mail address: e4602@mosk.tytlabs.co.jp (M. Hatanaka).

0021-9517/$ - see front matter © 2009 Elsevier Inc. All rights reserved.
doi:10.1016/j.jcat.2009.06.005

video images clearly captured the decrease in Pt particle size with time under an oxidative atmosphere at 1093 K [31].

From these results it can be expected that oxidized Pt will exist as a monolayer on the surface of CeO_2-based oxide supports after treatment in an oxidative atmosphere at high temperature. However, complete evidence of this phenomenon is not yet available. In the present study, we focused on the oxidation state and nanostructure of Pt on the surface of a CeO_2-based oxide support using XPS and TEM. XPS is more surface-sensitive than XAFS, and advanced high-resolution TEM can capture direct evidence of the Pt nanostructure that forms Pt–O–Ce bonds. We investigated whether reversible changes in the Pt oxidation state and nanostructure occur in sequentially oxidized, reduced, and re-oxidized Pt on a CeO_2-based support at high temperature.

2. Experimental

2.1. Support and catalyst preparation

In previous studies [27,30,31], 55 wt.% CeO_2 containing CeO_2–ZrO_2–Y_2O_3 (CZY) was used as the CeO_2-based support; however, the composition of primary particles of this material varies somewhat. Use of such heterogeneous material as a support for XPS Pt oxidation analysis would yield complicated results because the Pt oxidation states on Ce-rich and Zr-rich domains must be different. Thus, a support of simple composition is desirable to avoid ambiguity due to local heterogeneity in the support, and pure CeO_2 is ideal for this purpose. However, in principle, primary particles of pure CeO_2 treated at high temperature agglomerate to larger particles because pure CeO_2 is not thermally stable under these conditions. Therefore, CeO_2–Al_2O_3 was used as the support. Under an oxidative atmosphere, Al_2O_3 does not react with CeO_2 in the solid phase below 1273 K and is located at the grain boundaries of CeO_2 particles. Thus, Al_2O_3 acts as a diffusion barrier that restricts the contact point of primary CeO_2 particles and inhibits CeO_2 particle growth [24]. The support consisted of 89 wt.% CeO_2 and 11 wt.% Al_2O_3, and hereafter the CeO_2–Al_2O_3 support is denoted as CA. The CA support was prepared using the following precipitation method. Certain amounts of $Ce(NO_3)_3{\cdot}6H_2O$ and $Al(NO_3)_3{\cdot}9H_2O$ (Wako Pure Chemicals) were dissolved in ion-exchanged water and ammonia solution was added. The precipitated material was dried at 673 K for 5 h, calcined at 873 K for 5 h, and finally fired at 1073 K for 5 h in air in an ADVANTEC KM-420 muffle furnace. For comparison, a pure Al_2O_3 support was prepared using a similar method, except no $Ce(NO_3)_3{\cdot}6H_2O$ was included. The specific surface area of the CA and pure Al_2O_3 supports was 55 and 101 m^2/g, respectively, as determined by the BET one-point method using a Microdata Microsorp 4232II instrument.

Pt/CA and Pt/Al_2O_3 catalysts were prepared by conventional wet impregnation of the support powders with $Pt(NH_3)_2(NO_2)_2$ nitric acid solution (Tanaka Kikinzoku Kogyo K.K.). The Pt loading on the catalysts was controlled at 1.5 wt.%. The Pt-impregnated powders were dried at 393 K overnight and calcined at 773 K for 2 h in a muffle furnace. Then the powders were pressed into disks, crushed, and sieved to yield particles of 0.5–1.0 mm in diameter. These samples are referred to as fresh catalysts.

2.2. Catalyst treatments

Samples of 9 g of fresh catalysts were heated from room temperature to 1073 K under a flow of air (1000 ml/min) over a period of 1 h and maintained under these conditions for 5 h, then cooled to room temperature in flowing air to maintain the oxidation state of Pt. The catalysts treated under these oxidative conditions are referred to as oxidized catalysts.

Samples of 6 g of the oxidized catalysts were heated from room temperature to 873 K under a flow of 3% H_2/N_2 (1000 ml/min) over a period of 1 h and maintained under these conditions for 30 min, then cooled to room temperature under the H_2/N_2 flow to maintain the oxidation state of Pt. The catalysts treated under these reductive conditions are referred to as reduced catalysts.

Samples of 3 g of the reduced catalysts were further subjected to the same treatment as for the oxidized catalysts to yield re-oxidized catalysts.

2.3. Catalyst characterization

Pt in the oxidized, reduced, and re-oxidized catalysts was characterized using the following methods.

2.3.1. Pt particle diameter

The Pt particle diameter was quantified using CO pulse adsorption and XRD methods. CO adsorption measurements were performed using an OHKURA RIKEN prototype low-temperature CO adsorption apparatus [27]. A sample of 0.02 g of the catalyst was placed in a sample cell and pretreated according to the procedure established by the Catalysis Society of Japan. First, the catalyst was heated to 673 K in a flow of pure O_2 (20 ml/min) and maintained under the same conditions for 15 min, then the gas flow was changed to 20 ml/min pure He for 10 min, followed by 20 ml/min pure H_2 for 15 min to convert PtO_x into metallic Pt. Finally, the gas flow was changed back to 20 ml/min pure He for 10 min. The catalyst was then cooled to 195 K under the pure He flow using a dry ice/ethanol refrigerant to prevent CO adsorption on the CA support. Then, 0.75 μmol/pulse CO was injected into the catalyst under the He flow until the CO content in the outlet gas reached a constant value. The amount of CO adsorbed was calculated as the difference between the total amount injected and the sum of all CO detected in the outlet gas. The Pt particle diameter was estimated assuming that one CO molecule adsorbed onto each Pt atom on the surface of hemispherical Pt particles [27,32].

XRD measurements of the catalysts after the CO adsorptions were performed on a Bruker AXS D8 Advanced powder X-ray diffractometer using Cu K_α radiation ($\lambda = 0.1541$ nm) operated at 35 kV and 40 mA with a super-speed VANTEC-1 detector. Data were recorded in the 2θ range from 35° to 45° with an angular step size of 0.014° and a counting time of 1 s/step. The Pt particle diameter (D nm) was calculated from the width at half-height (B) of the Pt(1 1 1) diffraction line using the Scherrer equation $D = K\lambda/B\cos\theta$ ($K = 0.9$).

2.3.2. Analysis of the Pt oxidation state

XPS analysis of the oxidation state of supported Pt was carried out in two independent experiments. In the first experiment, the Pt oxidation state was measured for pulverized samples of the oxidized, reduced, and re-oxidized Pt/CA and Pt/Al_2O_3 catalysts without further treatment. An ULVAC-PHI PHI-Quantera SXM XPS system was used for this analysis with monochromatic Al K_α X-rays (1486.6 eV) at ambient temperature [33]. The electron escape depth and diameter of the analysis spot were approximately 2 nm and 100 μm, respectively. In the second experiment, changes in the Pt oxidation state were observed for the pre-reduced Pt/CA catalyst after sequential in-situ re-oxidizing treatment at 673, 873, and 1073 K for 10 min under 20% O_2/N_2 with an O_2 pressure of 0.05 MPa using the treatment chamber adjacent to an ULVAC-PHI PHI-5500MC XPS system. This experimental set-up allows direct transfer of treated catalysts from the treatment chamber to the measurement chamber, preventing catalyst exposure to room air. In this case, Mg K_α (1253.6 eV) radiation was used, and the electron escape depth and diameter of the analysis spot were approximately 2 nm and 800 μm, respectively. In both analyses, the Pt

binding energy (BE) was calibrated using the C 1s (284.5 eV) peak. The raw spectra were deconvoluted by curve fitting of the Gaussian distribution profiles. Pt $4f_{7/2}$ and $4f_{5/2}$ binding energies and the abundance of different Pt oxidation states were obtained from the corresponding positions and areas in the deconvoluted spectra.

2.3.3. Pt configuration measurements

Two different TEM systems were used to determine the Pt configuration in the Pt/CA and Pt/Al_2O_3 catalysts. A JEOL JEM-200CX microscope operated at an accelerating voltage of 200 kV was used to analyze the oxidized, reduced, and re-oxidized catalysts. In this case, TEM images were captured using the bright field (BF) mode. Further investigations of the re-oxidized Pt/CA catalyst were carried out using a JEOL JEM-2100F instrument operated at 200 kV. This system is equipped with a high-angle annular dark field (HAADF) image mode [34,35] for spherical aberration-corrected scanning transmission electron microscopy (C_s-corrected STEM) [36]. HAADF images are effective for delineating the Pt position on the CA support, because the heavier atom exhibits bright contrast in this mode, whereas it has dark contrast in the conventional BF mode [37]. Resolution of the C_s-corrected STEM was approximately 0.2 nm. The combination of HAADF and C_s-corrected STEM techniques provides easy detection of the nanostructure of Pt on the CA support. Each TEM system was equipped with energy-dispersive X-ray spectroscopy (EDS) capability to determine the chemical composition of local spots in the catalyst. The oxidized, reduced, and re-oxidized Pt/CA catalysts were pulverized using an agate mortar, sonicated in ethanol, and deposited on lacey carbon on copper grids for analysis.

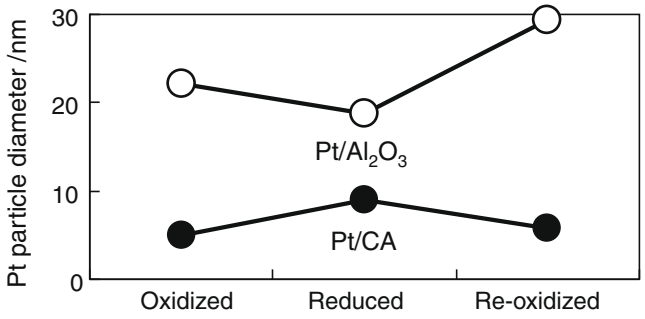

Fig. 1. Pt particle diameter for oxidized, reduced, and re-oxidized Pt/CA and Pt/Al_2O_3 catalysts according to CO adsorption data.

2.4. Thermodynamic calculations

In addition to the above experiments, thermodynamic calculations were carried out to identify the thermodynamic stability of the Pt oxidation state in the absence of interaction between Pt and the support. The commercial software HSC Chemistry® (Outokumpu Research Oy.) was used to compute Gibbs free energy changes (ΔG_T^0) at 673, 873, and 1073 K for PtO and PtO_2 formation from metallic Pt and O_2 gas. Comparison of the XPS results and thermodynamic calculations allows deduction of the interaction between Pt and the CA support.

3. Results and discussion

3.1. Pt dispersion following oxidative and reductive treatments

In previous XAFS analyses of sintering inhibition and redispersion of Pt on ceria-based oxide supports [27,30,31], CZY and commercial Al_2O_3 were used as the supports, which differ from the support used in the present investigation. Thus, before evaluating the Pt oxidation state and its nanostructure from XPS or C_s-corrected STEM results, it must be confirmed whether the CA support can inhibit Pt sintering compared to the Al_2O_3 support and if Pt agglomerates on the CA support can be redispersed under oxidative conditions. To evaluate inhibition of Pt sintering and redispersion of agglomerated Pt particles on the CA support under a heated oxidative atmosphere, the Pt particle size on oxidized, reduced, and re-oxidized Pt/CA and Pt/Al_2O_3 catalysts was evaluated by CO adsorption, XRD, and TEM methodologies.

Fig. 1 shows the Pt particle diameter for the oxidized, reduced, and re-oxidized catalysts estimated from CO adsorption data. The Pt particle diameter for the oxidized Pt/CA catalyst is 5 nm, whereas the Pt particle diameter for the oxidized Pt/Al_2O_3 catalyst is 22 nm. The Pt particle diameter of 5 nm for oxidized Pt/CA increased to 9 nm on reduction, and decreased to 6 nm on re-oxidation. In contrast, the Pt particle diameter for the reduced Pt/Al_2O_3 catalysts is 19 nm and increased to 29 nm on re-oxidation.

Fig. 2 shows XRD patterns for oxidized, reduced, and re-oxidized Pt/CA and Pt/Al_2O_3 catalysts following the CO adsorptions. The diffraction lines in each pattern at approximately 39.8° are attributed to Pt(111) (PDF#4-802 $2\theta = 39.763°$), because Pt species must be reduced into metallic state during the CO adsorption pretreatment. The intensity of Pt(111) diffraction lines was lower for Pt/CA than for Pt/Al_2O_3. The large difference in Pt(111) peak intensity between Pt/CA and Pt/Al_2O_3 catalysts suggests that the num-

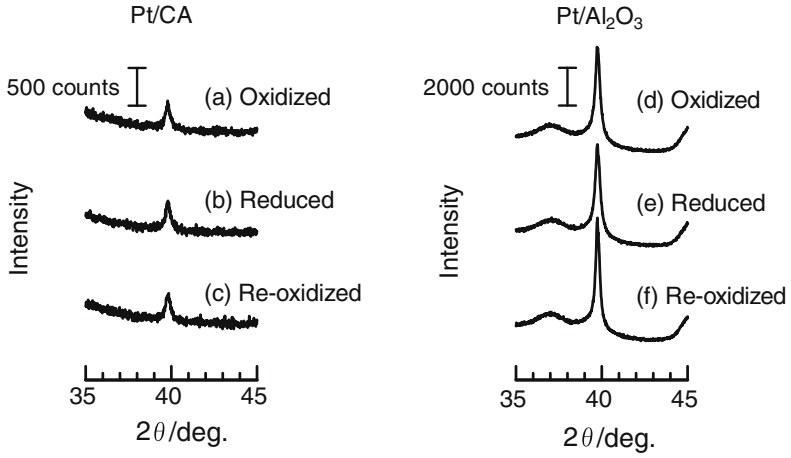

Fig. 2. XRD patterns for oxidized, reduced, and re-oxidized Pt/CA and Pt/Al_2O_3 catalysts following CO adsorption.

ber of agglomerated Pt particles on Pt/CA was less than that on Pt/Al_2O_3, whereas the diffraction intensity reflects both the number of agglomerated Pt particles and the X-ray absorption coefficient for the support elements. The Pt particle diameter was calculated for each catalyst according to the Scherrer equation using the Pt(1 1 1) diffraction lines in Fig. 2 and is summarized for the treatments in Fig. 3. The variations in Pt particle diameter on Pt/Al_2O_3 are almost the same as in Fig. 1; i.e., the Pt particle diameter of 19 nm for oxidized and reduced Pt/Al_2O_3 increased to 24 nm on re-oxidation. The Pt particle diameter of the oxidized Pt/CA catalyst shown in Fig. 3 was 24 nm and was stable on reductive and re-oxidative treatments, whereas the diameter shown in Fig. 1 reversibly changed on treatment. For Pt/CA, CO adsorption data yielded a smaller Pt diameter than the XRD data, whereas the diameter on Pt/Al_2O_3 was almost the same for both methods. The Pt particle diameter deduced from CO adsorption data reflects smaller Pt particles, whereas the diameter deduced from XRD data reflects larger particles if Pt exists as smaller and larger particles. Thus, the discrepancy in Pt particle diameter on Pt/CA for CO adsorption and XRD data suggests that Pt must be distributed on this catalyst as smaller and larger particles.

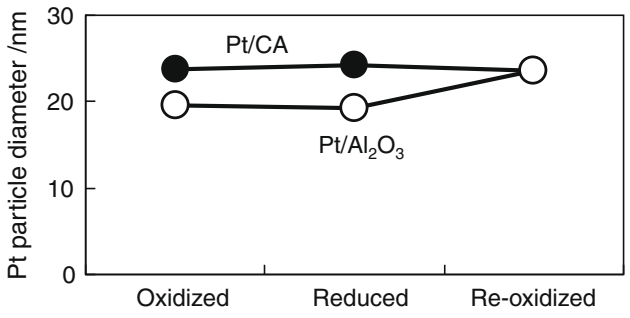

Fig. 3. Pt particle diameter for oxidized, reduced, and re-oxidized Pt/CA and Pt/Al_2O_3 catalysts according to XRD data.

Fig. 4 shows BF TEM images of oxidized, reduced, and re-oxidized Pt/CA and Pt/Al_2O_3 catalysts. The magnification of these images was adjusted to focus on any large Pt particles predicted from the XRD data. The dark spots (indicated by white arrows) of several 10 nm in diameter are clearly evident for each Pt/Al_2O_3 catalyst and the size of these spots matches the Pt particle diameters shown in Figs. 1 and 3. However, the dark contrast of the CA support made it impossible to identify any large Pt particles in these images because the atomic number of Ce is 58 whereas that of Al

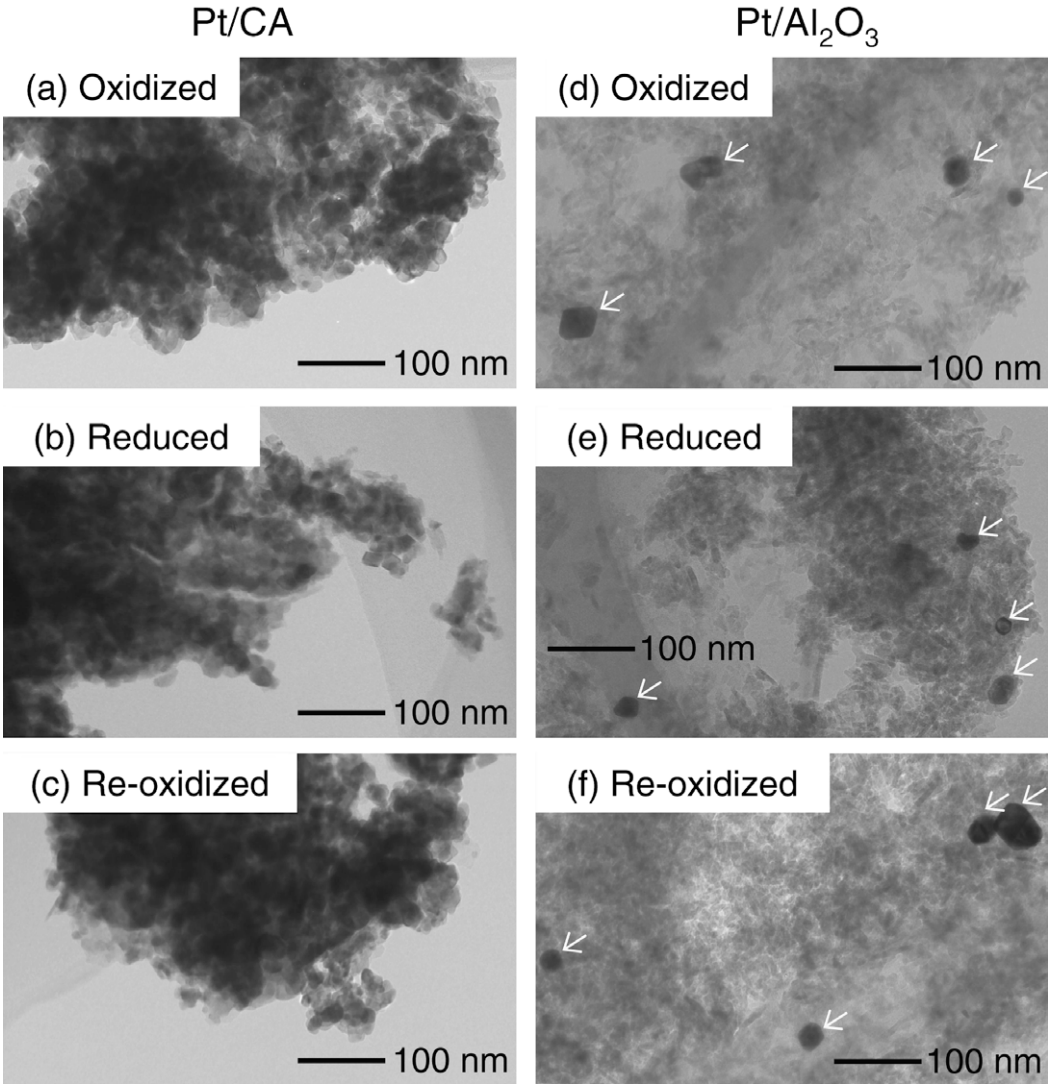

Fig. 4. Low-magnification TEM images of oxidized, reduced, and re-oxidized Pt/CA and Pt/Al_2O_3 catalysts. The white arrows indicate Pt particles.

is 18. CeO_2 agglomerates cannot transmit TEM electron beams, and thus observation of large Pt particles was hindered by the strong contrast for the CeO_2 support [38].

Fig. 5 shows higher-magnification TEM images of these catalysts. A number of small Pt particles of 1–2 nm in diameter (indicated by black arrows) are evident on the reduced Pt/CA catalyst (Fig. 5b), whereas no small Pt particles are observed in the other five TEM images. Small Pt particles of 1–2 nm in diameter are the predominant configuration in the reduced Pt/CA catalyst and they reversibly change on oxidative and reductive treatments. In contrast, larger Pt particles of several 10 nm in diameter are the principal configuration in the Pt/Al_2O_3 catalyst and these do not change on treatment.

The CO adsorption, XRD, and TEM data confirm that Pt sintering on the CA support was inhibited compared to the Al_2O_3 support under oxidative conditions at 1073 K, and smaller Pt particles on the CA support redispersed under oxidative treatment, even if they agglomerated under reductive conditions at 873 K. Thus, further characterization of the Pt/CA and Pt/Al_2O_3 catalysts was carried out to determine the Pt oxidation state and nanostructure on

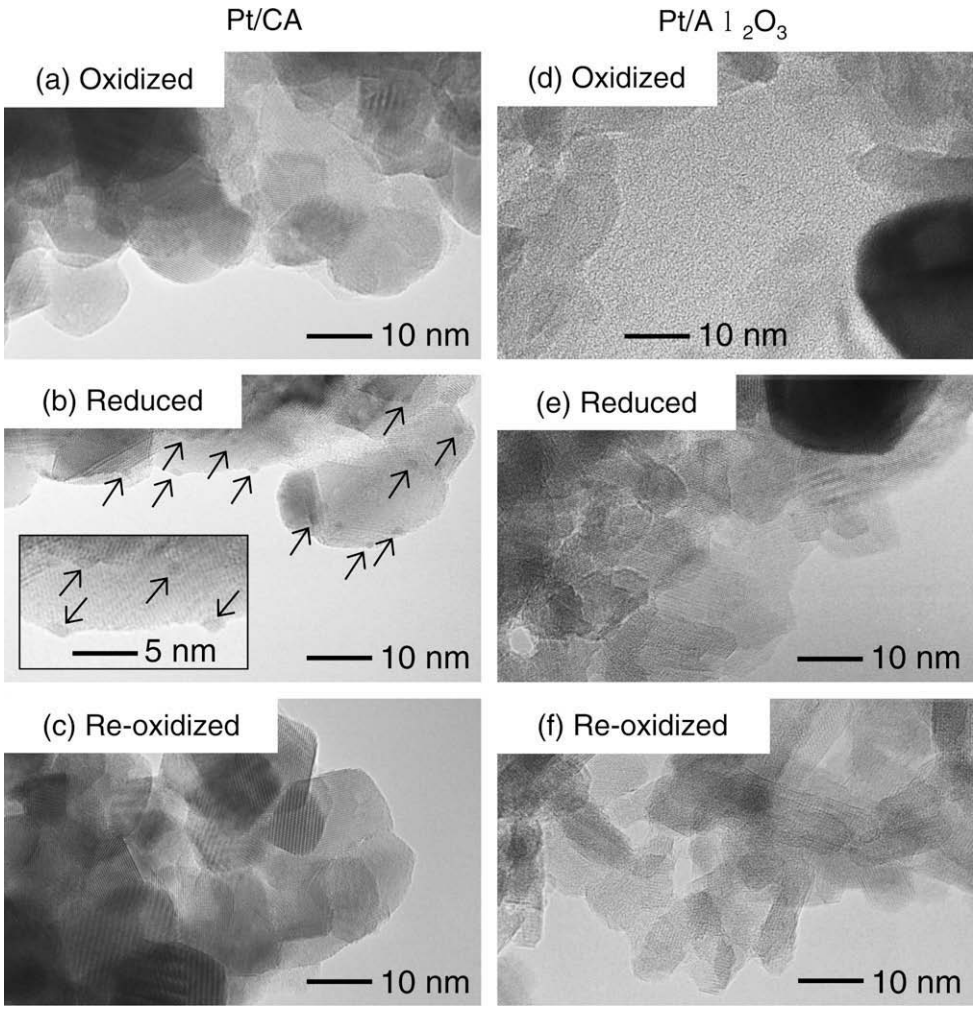

Fig. 5. High-magnification TEM images of oxidized, reduced, and re-oxidized Pt/CA and Pt/Al_2O_3 catalysts. The inset in (b) is a magnified image showing Pt nanoparticles on the reduced Pt/CA catalyst. The black arrows indicate Pt particles.

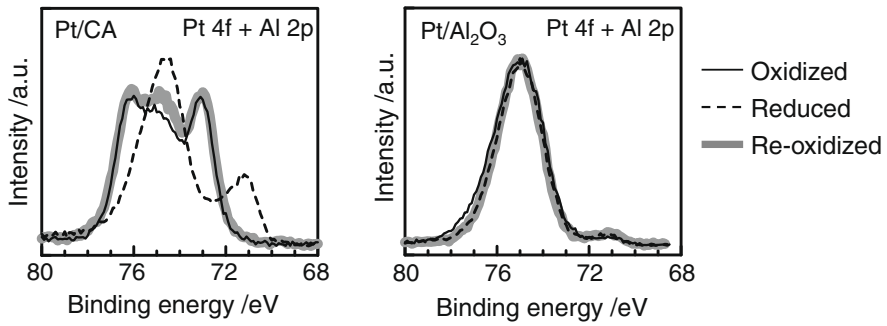

Fig. 6. Pt 4f and Al 2p XPS spectra of oxidized, reduced, and re-oxidized Pt/CA and Pt/Al_2O_3 catalysts.

oxidative and reductive treatments, with a focus on smaller Pt particles.

3.2. Pt oxidation state on oxidative and reductive treatments

Fig. 6 shows Pt 4f and Al 2p XPS spectra of the oxidized, reduced, and re-oxidized Pt/CA and Pt/Al_2O_3 catalysts. The Pt/CA peak positions reversibly changed on oxidizing, reducing, and re-oxidizing treatments, whereas the Pt/Al_2O_3 peaks were stable. The XPS spectrum for the reduced Pt/CA catalyst had two peaks at 71.1 and 74.5 eV. According to the literature [39], the BE for Pt^0 (metal) $4f_{7/2}$ and $4f_{5/2}$ is 71.1 and 74.4 eV, respectively, and that for Al 2p is 74.5–75.5 eV. Thus, the peak at 71.1 eV for the reduced Pt/CA catalyst can be assigned to Pt^0 $4f_{7/2}$ and that at 74.5 eV as an overlap of peaks for Pt^0 $4f_{5/2}$ and Al 2p. The spectra for the oxidized and re-oxidized Pt/CA catalysts had three peaks at 73.0, 75.0, and 76.3 eV. Pozdnyakova et al. [38] reported Pt^{2+} peaks at +1.0–1.8 or +2.4–3.0 eV and Pt^{4+} peaks at +3.6–4.5 eV relative to the peak position of Pt^0. Thus, the first and third peaks at 73.0 and 76.3 eV for the oxidized and re-oxidized Pt/CA catalysts were shifted by +1.9 eV from Pt^0 $4f_{7/2}$ and $4f_{5/2}$(71.1 and 74.4 eV) for the reduced catalyst, and the second peak at 75.0 eV corresponds to Al 2p. Based on this assignment, the components with BE of 73.0 and 76.3 eV were thought to correspond to the +2 rather than the +4 oxidation state of Pt, and we denote these as oxidized $Pt_{+1.9eV}$.

For more quantitative analysis of changes in the Pt oxidation state on oxidative and reductive treatment, XPS deconvolution was carried out. The raw data and deconvolution results for Pt/CA and Pt/Al_2O_3 catalysts are summarized in Fig. 7. Among the six raw spectra, the reduced Pt/CA XPS spectrum requires an unanticipated Pt oxidation state, positioned between Pt^0 and oxidized $Pt_{+1.9eV}$, for successful deconvolution. We call this oxidized $Pt_{+1.0eV}$, with $4f_{7/2}$ and $4f_{5/2}$ BE of 72.1 and 75.4 eV, respectively. Two reasons can be proposed for the presence of oxidized $Pt_{+1.0eV}$ on the reduced Pt/CA catalyst. One is that strong interaction between Pt and the CA support inhibited full metallation of supported Pt, particularly at the interface between Pt particles and the support, because oxidized $Pt_{+1.0eV}$ cannot be observed on the Al_2O_3 support, which has weak interaction with Pt. The other is that Pt was oxidized on exposure to air at room temperature following reductive treatment in the furnace, and was metastable under the ultra-high vacuum conditions in the XPS chamber, because the majority of Pt on the CA support existed as small particles with a large surface area, as described in Section 3.1. Further investigations are required to elucidate the source of this phenomenon; however, we believe that the former is more likely than the latter. The Pt $4f_{7/2}$ and $4f_{5/2}$ BE values for Pt^0, oxidized $Pt_{+1.0eV}$, and oxidized $Pt_{+1.9eV}$ are summarized in Table 1.

Peak deconvolution for all six XPS spectra was performed assuming that four different chemical species were present: Pt^0, oxidized $Pt_{+1.0eV}$, oxidized $Pt_{+1.9eV}$, and Al 2p. The abundance of Pt in these different oxidation states is shown in Fig. 8 for oxidative and reductive treatments. For the oxidized and re-oxidized Pt/CA catalysts, oxidized $Pt_{+1.9eV}$ was the dominant chemical species, whereas Pt^0 was the principal species for the reduced catalyst. Oxidized $Pt_{+1.9eV}$ might form a Pt–O–Ce bond that inhibits Pt sintering under heated oxidative conditions. The abundance of Pt in different oxidation states changed reversibly on oxidative and reductive treatments. These phenomena can be attributed to the strong interaction between Pt and the CA support under heated oxidative conditions, as predicted by XAFS data in previous studies [27,30,31]. In contrast, Pt^0 was the dominant species for all Pt/Al_2O_3 catalysts. The Pt^0 abundance did not decrease, even when the Pt/Al_2O_3 catalyst was treated under heated oxidative conditions. This is in good agreement with our previous results [27,30,31] indicating a lack of strong interaction between Pt and Al_2O_3 supports under heated oxidative conditions, with no rigid Pt–O–Al bond formed.

Further investigations in the present study were focused on the Pt/CA catalyst, because the results demonstrated a lack of strong

Table 1
Pt binding energies of different Pt oxidation states in Pt/CA and Pt/Al_2O_3 catalysts.

Pt oxidation state	Pt binding energy (eV)	
	$4f_{7/2}$	$4f_{5/2}$
Pt^0	71.1	74.4
$Pt_{+1.0eV}$	72.1	75.4
$Pt_{+1.9eV}$	73.0	76.3

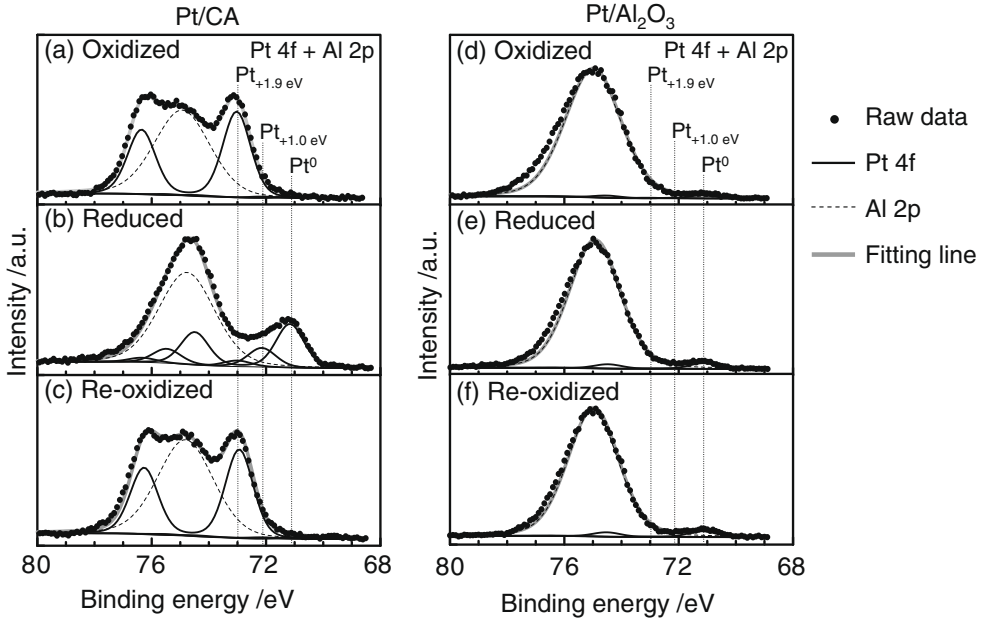

Fig. 7. Pt 4f and Al 2p XPS spectra and deconvolution results for oxidized, reduced, and re-oxidized Pt/CA and Pt/Al_2O_3 catalysts.

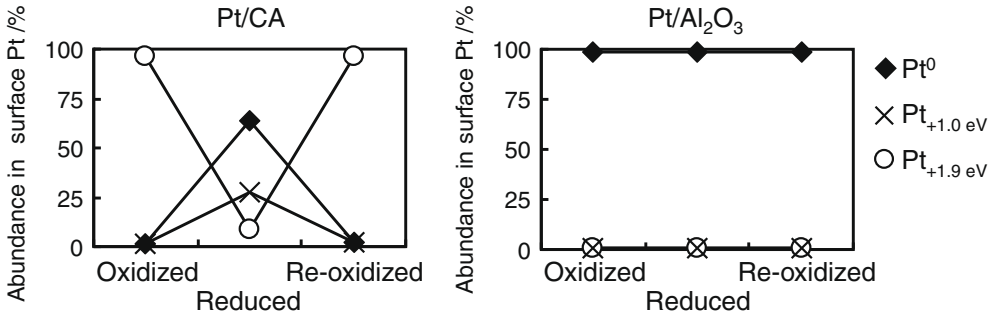

Fig. 8. Abundance of Pt in different oxidation states on oxidized, reduced, and re-oxidized Pt/CA and Pt/Al_2O_3 catalysts.

interaction between Pt and the Al_2O_3 support under oxidative conditions at high temperature, and the primary aim was to account for the oxidation state and nanostructure of Pt on strong interaction with CeO_2.

3.3. Change in Pt oxidation state on heated oxidative treatment

Previous XAFS studies [27,30,31] revealed that Pt was stabilized by Pt–O–Ce bonds on a CZY support under an oxidative atmosphere at high temperature. However, there are no reports on the Pt oxidation state in relation to the oxidative treatment temperature. Pt must be oxidized to form Pt–O–Ce bonds for inhibition of Pt sintering under a heated oxidative atmosphere. Thermodynamic calculations using HSC Chemistry® suggested that PtO and PtO_2 formations from metallic Pt and O_2 gas were restricted during oxidative treatment at higher temperatures if there is no interaction between Pt and the support, because ΔG_T^0 was −13.3, 2.6, and 17.9 kJ/mol Pt for Eq. (1) and −15.3, 14.4, and 41.7 kJ/mol Pt for Eq. (2) at 673, 873, and 1073 K, respectively.

$$\mathrm{Pt} + \frac{1}{2}\mathrm{O_2} \rightarrow \mathrm{PtO} \quad (1)$$

$$\mathrm{Pt} + \mathrm{O_2} \rightarrow \mathrm{PtO_2} \quad (2)$$

Thus, the Pt oxidation state was evaluated for different oxidative treatment temperatures.

The Pt oxidation state of the reduced Pt/CA catalyst before and after re-oxidative treatments at 673, 873, and 1073 K was analyzed using an XPS system equipped with a treatment chamber, as described in the Experimental section. As indicated by the dots in Fig. 9, the XPS spectral shape changed with the treatment temperature. Spectral deconvolution was carried out assuming that four chemical species were present: Pt^0, oxidized $Pt_{+1.0eV}$, oxidized $Pt_{+1.9eV}$, and Al 2p. The deconvolution results are also shown in Fig. 9. The abundance of Pt in different oxidation states was determined from the deconvolution results and is summarized in Fig. 10. Similar to the result in Fig. 8, Pt^0, oxidized $Pt_{+1.0eV}$, and oxidized $Pt_{+1.9eV}$ were present in the reduced Pt/CA catalyst at abundance ratios of 42%, 41%, and 17%, respectively. The Pt^0 abundance decreased to zero when the Pt/CA catalyst was re-oxidized at $\geqslant$673 K. The abundance of oxidized $Pt_{+1.0eV}$ gradually decreased with increasing re-oxidizing temperature. In contrast, the abundance of oxidized $Pt_{+1.9eV}$ monotonically increased with the treatment temperature. After the Pt/CA catalyst was re-oxidized at 1073 K, the abundance of oxidized $Pt_{+1.9eV}$ was approximately 96%.

The discrepancy between thermodynamic predictions and the experimental results can be attributed to the strong interaction between oxidized Pt and CeO_2 under oxidative conditions at high temperatures, i.e., the formation of a Pt–O–Ce bond decreases the total energy of the whole Pt/CA catalyst system and stabilizes Pt on the surface of CA support.

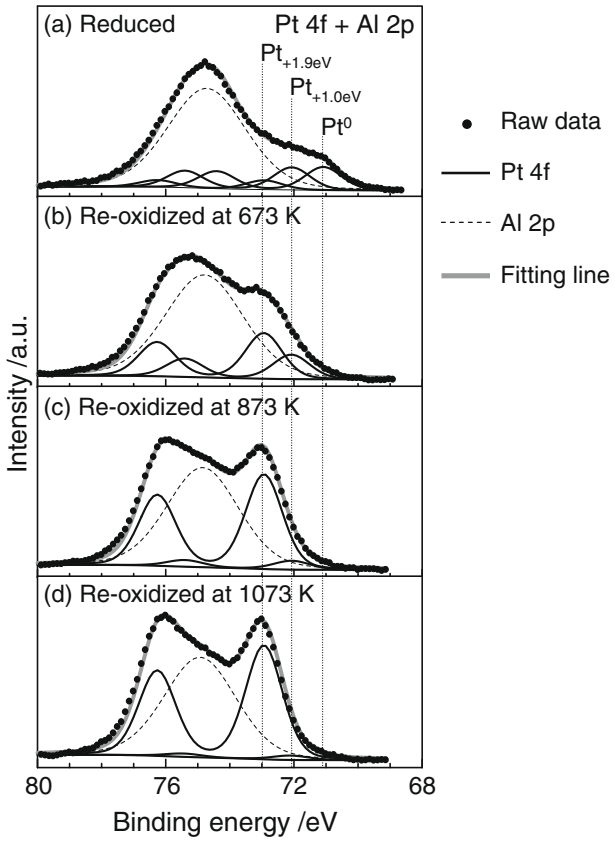

Fig. 9. Pt 4f and Al 2p XPS spectra and deconvolution results for a reduced Pt/CA catalyst before and after re-oxidative treatment at 673, 873, and 1073 K.

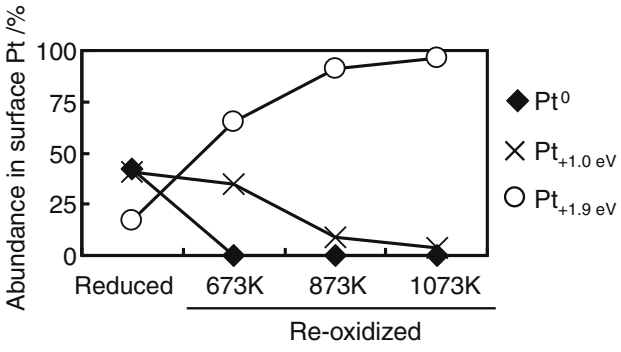

Fig. 10. Abundance of Pt in different oxidation states on a reduced Pt/CA catalyst before and after re-oxidative treatment at 673, 873, and 1073 K.

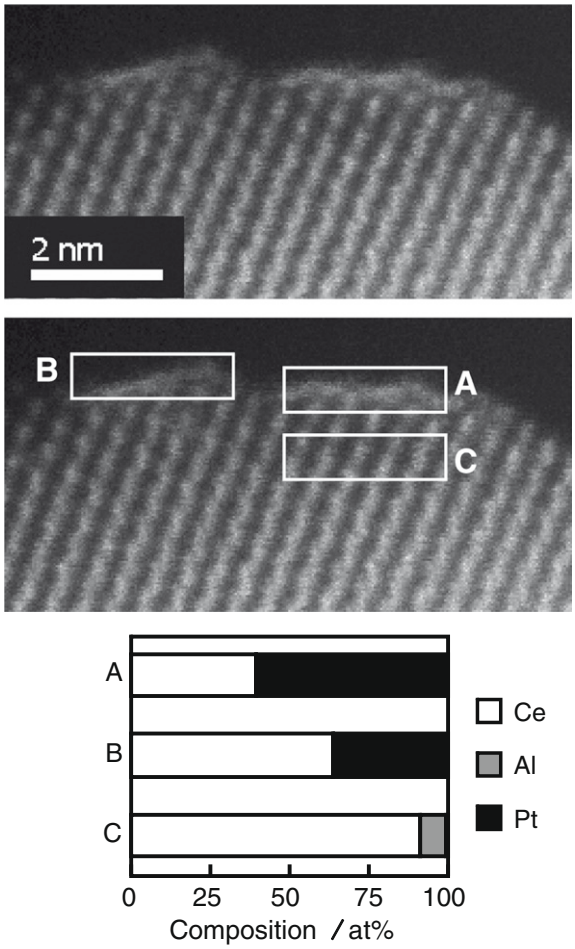

Fig. 11. HADDF image of a re-oxidized Pt/CA catalyst captured by STEM with C_s correction and composition of areas A, B, and C according to EDS analysis.

3.4. Pt nanostructure of re-oxidized Pt/CA

As shown in Fig. 5, no Pt was detected on the oxidized and re-oxidized Pt/CA, whereas Pt particles of 1–2 nm were observed on the reduced catalyst. However, the average Pt particle diameter deduced from CO adsorption was ~5 nm for oxidized and re-oxidized Pt/CA catalysts, which is approximately half of the diameter deduced for the reduced catalyst (9 nm), as described in Section 3.1. Thus, we attempted to identify the Pt nanostructure in the oxidized Pt/CA catalysts, which could not be observed using conventional TEM. Fig. 11 presents a HAADF image of the re-oxidized Pt/CA catalyst captured by STEM with C_s correction. Bright layers of 0.1–0.2 nm in thickness are overlaid on some portions of the top surface of the CA support. The lattice fringe observed for support particles indicates that this CA domain is CeO_2 crystals and not Al_2O_3. As shown in the composition bar graph in Fig. 11, the Pt concentration in areas A and B on the surface of the CA support was approximately 60 and 35 at.%, respectively, whereas no Pt was detected in area C located in the bulk of the CA support. Therefore, the thin bright layers were Pt and they existed on the top surface of CeO_2 particles in the CA support. This Pt should be oxidized $Pt_{+1.9eV}$ according to XPS spectra. In other words, this Pt is probably oxidized and interacts with the CeO_2-based support; i.e., oxidized Pt forms a Pt–O–Ce bond and exists as a monolayer on the surface of the support, as expected from previous XAFS investigations [27,30,31].

3.5. Summary of the Pt oxidation state and nanostructure

Based on the CO adsorption, TEM, and XPS data shown in Figs. 1,5,8, and 11, the Pt oxidation state and nanostructure on the Pt/CA catalyst can be deduced, as shown in Fig. 12a. In this case, following oxidative treatment at 1073 K, oxidized $Pt_{+1.9eV}$ spreads as a monolayer on the surface of CeO_2 in the CA support. When the Pt/CA catalyst was subjected to reductive conditions at 873 K, oxidized $Pt_{+1.9eV}$ was reduced to oxidized $Pt_{+1.0eV}$ and metallic Pt and these Pt species changed from a monolayer to agglomerated particles. It is possible that oxidized $Pt_{+1.0eV}$ atoms might exist at the interface between the support and Pt particles, and metallic Pt atoms might be present on the layer of oxidized $Pt_{+1.0eV}$ atoms, as described in Section 3.2. Following re-oxidative treatment at 1073 K, the Pt oxidation state and nanostructure reverted to those of the oxidized catalyst, i.e., oxidized $Pt_{+1.9eV}$ existed as a redispersed monolayer on the support surface. The Pt oxidation state and configuration on the Al_2O_3 support can be deduced, as shown in Fig. 12b, by considering the CO adsorption result shown in Fig. 1, the XRD result shown in Fig. 3, the TEM image shown in Fig. 4, and the XPS data shown in Fig. 8. In this case, following oxidative treatment at 1073 K, Pt atoms might form Pt metal particles on the Al_2O_3 support. After subsequent reductive treatment at 873 K, the Pt oxidation state and configuration hardly changed compared to the oxidized catalyst. Pt metal particles agglomerated when this catalyst was re-oxidized at 1073 K, because the Pt oxidation state on the Al_2O_3 support was metallic even after oxidative treatment at 1073 K, and the Pt particle size was larger on re-oxidized Pt/Al_2O_3 than on the oxidized and reduced catalysts.

4. Conclusions

We determined changes in the Pt oxidation state and nanostructure on a CA support after oxidative and reductive treatments. From the results obtained in the present study, we can conclude

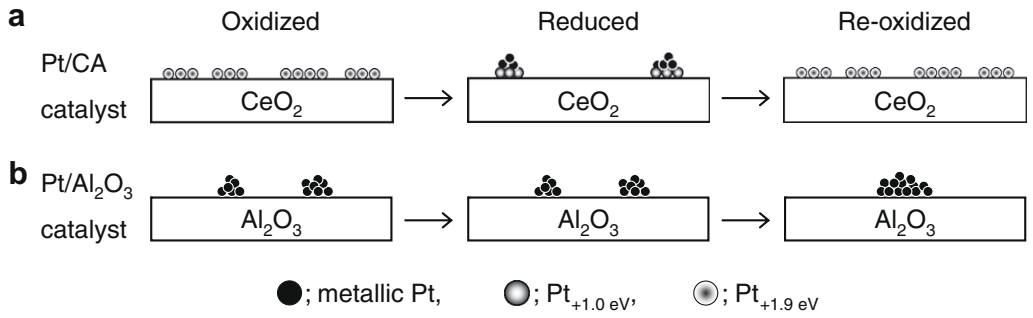

Fig. 12. Image of changes in the Pt oxidation state and nanostructure of Pt/CA and Pt/Al_2O_3 catalysts against oxidative, reductive, and re-oxidative treatments as determined from CO adsorption, XRD, TEM, and XPS analyses.

that a monolayer of Pt with a higher oxidation state than metallic Pt forms a complex oxide with Ce on the surface of the CA support, which inhibits Pt sintering and causes redispersion of Pt agglomerates under oxidative conditions. This Pt can be reversibly reduced to the metallic state, and it forms a complex oxide with the CeO_2-based support as the atmosphere fluctuates between reductive and oxidative conditions.

Acknowledgments

The authors gratefully acknowledge Mr. Eiji Okunishi of JEOL Ltd. for the JEM-2100F experiments, Mr. Noritomo Suzuki of TOYOTA Central R&D Labs Inc. for the JEM-200CX investigations, and Mr. Kazuhiko Dohmae of TOYOTA Central R&D Labs Inc. for discussions.

Appendix A. Supplementary data

Supplementary data associated with this article can be found, in the online version, at doi:10.1016/j.jcat.2009.06.005.

References

[1] S. Matsumoto, Catal. Today 90 (2004) 183.
[2] H.C. Yao, Y.F. Yao, J. Catal. 86 (1984) 254.
[3] M. Ozawa, M. Kimura, A. Isogai, J. Alloys Comp. 193 (1993) 73.
[4] Y. Nagai, T. Yamamoto, T. Tanaka, S. Yoshida, T. Nonaka, T. Okamoto, A. Suda, M. Sugiura, Catal. Today 74 (2002) 225.
[5] J.C. Summers, J.J. White, W.B. Williamson, SAE Tech. Paper 890794, 1989.
[6] R.J. Brisley, G.R. Chandler, H.R. Jones, P.J. Anderson, P.J. Shady, SAE Tech. Paper 950259, 1995.
[7] E. Jobson, O. Hjortsberg, S.L. Anderson, I. Gottberg, SAE Tech. Paper 960801, 1996.
[8] M.V. Twigg, N.R. Collins, D. Morris, R.J. Brisley, A.J. Ribeiro, G.D. Borgialli, SAE Tech. Paper 2000-01-3303, 2001.
[9] Y. Nishihata, J. Mizuki, T. Akao, H. Tanaka, M. Uenishi, M. Kumura, T. Okamoto, N. Hamada, Nature 411 (2002) 164.
[10] T. Yoshida, A. Sato, H. Suzuki, T. Tanabe, N. Takahashi, SAE Tech. Paper 2006-01-1061, 2006.
[11] N.R. Collins, M.V. Twigg, Top. Catal. 42/43 (2007) 323.
[12] S.Y. Christou, A.M. Efstathiou, Top. Catal. 42/43 (2007) 415.
[13] T. Tanabe, Y. Nagai, K. Dohmae, H. Sobukawa, H. Shinjoh, J. Catal. 257 (2008) 117.
[14] D.M. Fernandes, A.A. Neto, M.J.B. Cardoso, F.M.Z. Zotin, Catal. Today 133–135 (2008) 574.
[15] Y. Sakamoto, K. Higuchi, N. Takahashi, K. Yokota, H. Doi, M. Sugiura, Appl. Catal. B 23 (1999) 159.
[16] Y.F. Chu, E. Ruckenstein, J. Catal. 55 (1978) 281.
[17] I. Sushumna, E. Ruckenstein, J. Catal. 109 (1988) 433.
[18] M. Funabiki, T. Yamada, SAE Tech. Paper 881684, 1988.
[19] N. Miyoshi, S. Matsumoto, M. Ozawa, M. Kimura, SAE Tech. Paper 891970, 1989.
[20] E. Ruckenstein, B. Pulvermacker, J. Catal. 29 (1973) 224.
[21] B.K. Chakraverty, J. Phys. Chem. Solids 28 (1967) 2401.
[22] P. Wynblatt, N.A. Gjoostein, Prog. Solid State Chem. 9 (1975) 21.
[23] P.C. Flynn, S.E. Wanke, J. Catal. 34 (1974) 390.
[24] A. Morikawa, T. Suzuki, T. Kanazawa, K. Kikuta, A. Suda, H. Shinjoh, Appl. Catal. B 78 (2008) 210.
[25] H. Muraki, H. Sobukawa, M. Kimura, A. Isogai, SAE Tech. Paper 900610, 1990.
[26] E.C. Su, W.G. Rothschild, J. Catal. 99 (1986) 506.
[27] Y. Nagai, T. Hirabayashi, K. Dohmae, N. Takagi, T. Minami, H. Shinjoh, S. Matsumoto, J. Catal. 242 (2006) 103.
[28] A.F. Diwell, R.R. Rajaram, H.A. Shaw, T.J. Truex, Stud. Surf. Sci. Catal. 71 (1991) 139.
[29] L.L. Murrell, S.J. Tauster, D.R. Anderson, Stud. Surf. Sci. Catal. 71 (1991) 275.
[30] Y. Nagai, N. Takagi, Y. Ikeda, K. Dohmae, T. Tanabe, G. Guilera, S. Pascarelli, M. Newton, H. Shinjoh, S. Matsumoto, Stud. Surf. Sci. Catal. 172 (2007) 623.
[31] Y. Nagai, K. Dohmae, Y. Ikeda, N.I. Takagi, T. Tanabe, N. Hara, G. Guilera, S. Pascarelli, M.A. Newton, O. Kuno, H. Jiang, H. Shinjoh, S. Matsumoto, Angew. Chem., Int. Ed. 47 (2008) 9303.
[32] J.A. Anderson, R.A. Daley, S.Y. Christou, A.M. Efstathiou, Appl. Catal. B 64 (2006) 189.
[33] N. Takahashi, K. Dohmae, H. Sobukawa, H. Shinjoh, J. Chem. Eng. Jpn. 40 (2007) 741.
[34] E. Abe, A. Tsai, J. Non-Cryst. Solids 334–335 (2004) 198.
[35] M. Panjan, S. Šturm, P. Panjan, M. Čekada, Surf. Coat. Technol. 202 (2007) 815.
[36] S. Bals, B. Kabius, M. Haider, V. Radmilovic, C. Kisielowski, Solid State Commun. 130 (2004) 675.
[37] T. Akita, M. Okumura, K. Tanaka, M. Kohyama, M. Haruta, Catal. Today 117 (2006) 62.
[38] O. Pozdnyakova, D. Teschner, A. Wootsch, J. Kröhnert, B. Steinhauer, H. Sauer, L. Toth, F.C. Jentoft, A. Knop-Gericke, Z. Paál, R. Schlögl, J. Catal. 237 (2006) 1.
[39] J.F. Moulder, W.F. Stickle, P.E. Sobol, K.D. Bomben, Handbook of X-Ray Photoelectron Spectroscopy, 1992, p. 180.